photonics

MDPI

Article

Speckle Noise-Free Interconnective Holographic Projection

Hosung Jeon and Joonku Hahn *

School of Electronic and Electrical Engineering, Kyungpook National University, 80 Daehak-ro, Buk-gu, Daegu 41566, Republic of Korea
* Correspondence: jhahn@knu.ac.kr

Abstract: Generally, speckle noise is regarded as unavoidable in holographic projection, and it results from unexpected high spatial frequency components of diffracted light at the sharp edge of pixel openings in a spatial light modulator. Speckle noise typically reduces image contrast and degrades the image quality of the holographic projection. In this study, we propose a novel holographic optical interconnection method free of speckle noise in holographic projection. This optical interconnection is achieved by using a holographic optical element (HOE). The HOE is designed to reconstruct Gaussian beams with low divergence. These Gaussian beams become points which form target images at desired depths. Since the Gaussian beam from the HOE does not share the same position with other Gaussian beams, there is no interference at the projection image. Therefore, the image is composed of the points from the Gaussian beams and there is no reason for unexpected high spatial frequency noise to appear on the image. In this paper, we fabricate the HOE, produced with our specially manufactured hologram printer, where the directions of two Gaussian beams with low divergence are controlled by goniometers. We experimentally demonstrated a speckle noise-free interconnective holographic projection. Two images are successfully formed at different depths by optically connecting two points in pairs.

Keywords: optical interconnection; speckle reduction; holographic projection; hologram printer

check for updates

Citation: Jeon, H.; Hahn, J. Speckle Noise-Free Interconnective Holographic Projection. *Photonics* **2022**, *9*, 899. https://doi.org/10.3390/photonics9120899

Received: 21 October 2022
Accepted: 22 November 2022
Published: 24 November 2022

Publisher's Note: MDPI stays neutral with regard to jurisdictional claims in published maps and institutional affiliations.

Copyright: © 2022 by the authors. Licensee MDPI, Basel, Switzerland. This article is an open access article distributed under the terms and conditions of the Creative Commons Attribution (CC BY) license (https://creativecommons.org/licenses/by/4.0/).

1. Introduction

Holographic projection is a method to reconstruct the optical wave that forms target images in three-dimensional (3D) space using a hologram. This holographic projection has received great interest because it has been applied in many fields, such as image formation, optical information transfer, and beam shaping [1–4]. In holographic projection technology, 3D contents are generally displayed by modulating the phase of the optical wave [5–7]. The optical wave propagates to one depth and forms an image expected at the given depth. Then, it propagates to the next depth and forms an image correct to the depth. So, 3D contents are represented as a set of sliced images [8–10]. When a sliced image enters the eye of an observer, the observer perceives 3D objects. Depending on the depth at which the observer focuses, the image at one depth looks sharp, while the images at other depths are defocused. The accommodation effect makes the 3D contents natural to the observers.

In holographic projection, the hologram needs to project different images depending on the depth for displaying sliced images as 3D contents. For this purpose, whole optical waves forming these images are multiplexed in the hologram. An image formed at a given depth looks sharp in focus at that depth, but the images formed at other depths fade out. As the observer changes his eye focus, one image in focus gradually fades out, and another image fades in. At this time, the faded-out image does not disappear completely, and it becomes the noise of the faded-in image at different depths. So, the contrast of the image is reduced. Figure 1a shows that the optical wave passing through the hologram T, converges at a point on plane A, but diverges after passing through plane A. In other words, the optical wave converging at one point on plane A, diverges over a wide area on plane B, and this profile of diverging wave becomes noise. In plane B, each noise profile has a smooth

distribution, but due to the coherence of the light source, one diverging wave interferes with the others. It results in spackle noise with high spatial frequencies. Recently, for the reduction of such speckle noise, techniques for optimizing the holographic pattern with a camera, by capturing the image of each layer and comparing the target image with the captured image, are proposed [11]. However, while these methods reduce speckle noise and increase the contrast of holographic projection images, the speckle noise is fundamentally unavoidable because of the speckle noise from the coherence of the light source. The light is dominantly diffracted at the sharp edges of the pixel apertures, and there is no way to eliminate noise by using conventional methods [12].

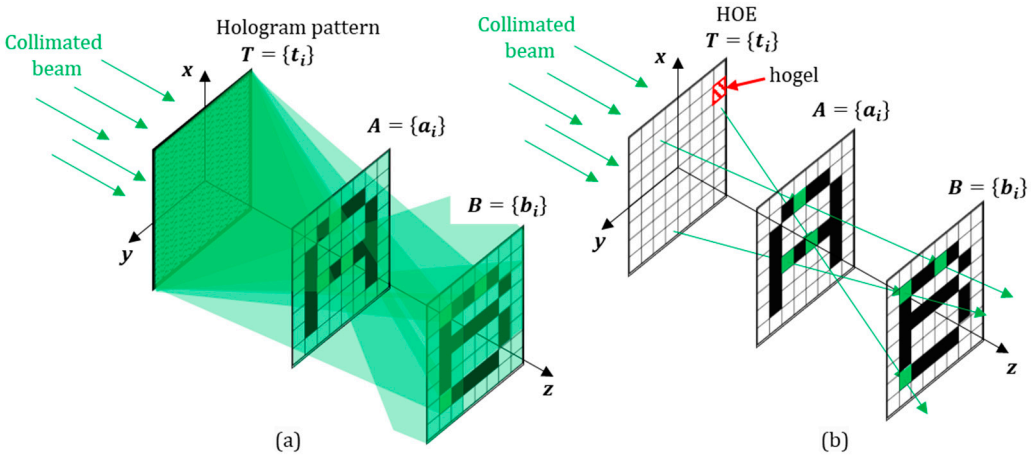


Figure 1. Conceptual scheme for holographic projections; (**a**) using conventional holographic projection and (**b**) the proposed speckle noise-free holographic projection.

Holographic optical interconnection is a technology that transmits optical power from one point on a plane to a specific point on another plane, by diffracting the waves on fringe patterns [13–15]. Here, the design of the fringe pattern determines the propagation direction of the diffracted wave. Techniques for generating fringe patterns using spatial light modulators (SLMs) actively change the directions of diffracted beams [16–18]. Dynamic optical interconnection is implemented using the SLM, which is used as a many-to-many switching technology in optical communication. Here, the waves are transmitted through optical fibers to increase the signal-to-noise ratio. A grin lens attached to the front of the optical fiber forms a Gaussian beam with low divergence.

In this paper, we propose a speckle noise-free interconnective holographic projection (IHP) based on holographic optical interconnection. The diffraction of the incident beam to the desired direction needs a short grating period. Usually, the SLM has a relatively large interval among pixels to achieve a high diffraction angle. So, we used a holographic optical element instead of the SLM to overcome the limitations of the diffraction angle. It is noted that the HOE contains the grating patterns on each hogel, which is recorded by interference between the reference beam and the signal beam. As shown in Figure 1b, a set of T hogels is recorded on the HOE for the IHP. The HOE grating determines the direction of rays, which present dots as images at each depth. This method has an advantage in signal contrast. The beam diameter of the ray changes slightly, since the beam from the single-mode fiber has a Gaussian profile. In addition, the collimated rays propagate in free space so that the speckle noise is not generated, and a high signal-to-noise ratio is achieved.

2. Fabrication of Holographic Optical Elements for Interconnective Holographic Projection

The HOE for interconnective holographic projection needs to have different gratings for individual hogels. We made a special hologram printer for recording the HOE and the concept of the printer is shown in Figure 2a. This hologram printer records the HOE at the interference between two collimated beams in a hogel. In the hologram printer, two collimators are placed on both sides of the HOE, where the upper collimator is for the

reference beam and the lower collimator is for the signal beam. The reference beam is fixed so that it always illuminates every hogel on the HOE in the same direction, as one collimated beam is used as a light source for the IHP. The reference beam is depicted as an arrow in $-k_y$, as shown in Figure 2b. On the other hand, the direction of the signal beam is changeable by a mechanical tilting stage, and the direction is depicted as vector $\vec{a_i b_i}$, tilted by θ, as shown in Figure 2b. The interference pattern from two beams is recorded on a hogel. Here, the origin of the tilting stage is placed at the same position of the hogel, and the signal beam points out the same hogel, independent of tilting angles of the stage. After recording one hogel, an xy-stage moves the HOE to record the next hogel.

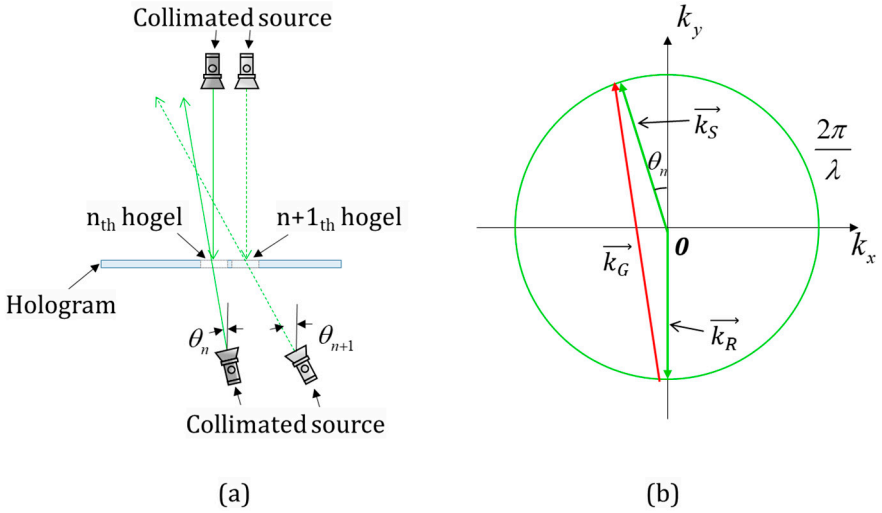


Figure 2. The proposed HOE generation method for IHP. (**a**) Hologram printer concept and (**b**) k-vector diagram at nth hogel.

For the nth hogel, the recorded linear grating is represented as grating vector $\vec{k_G}$, and is calculated as the difference between two- vectors of the signal and reference beam as follows:

$$\vec{k_G} = \vec{k_S} - \vec{k_R} \tag{1}$$

where $\vec{k_R}$ and $\vec{k_S}$ denote the reference and signal beams, respectively. Note that the vectors for both beams have the same length of $2\pi/\lambda$. The length of the grating vector is $2\pi/\Lambda$, where Λ represents the period of the grating. To make the diffraction efficiency of the volume grating high, the Bragg condition must be satisfied. The Q-factor indicates whether the material is operated in the Bragg condition [19]. If it must be larger than 2π, the Bragg condition is satisfied. The Q-factor is defined as follows:

$$\mathrm{Q} = \frac{2\pi\lambda T_m}{n\Lambda^2} \tag{2}$$

where T_m represents the thickness of the material, and n represents the refractive index of the material. From Equation (2), the thickness of the hologram material is obtained to satisfy the Bragg condition. In this study, the maximum tilting angle and the wavelength of the signal beam are 30-degrees and 532 nm, respectively. The grating pitch becomes the minimum when it is equal to the wavelength. Therefore, the minimum thicknesses of the hologram materials are smaller than 1 µm. Generally, the common hologram medium has a sufficient thickness of approximately 15 µm, making it suitable for the proposed holographic projection.

Figure 3 shows the system design and the realized hologram printer [20] for fabricating the HOE for a speckle noise-free IHP. In the signal arm, the signal beam is collimated and defined by a reflective collimator and a two-axis goniometer set, as shown in Figure 3a.

The reflective collimator is more suitable mounted on the goniometer than a refractive type one because the optical axis is folded. Two sets of two-axis linear stages are applied to both the reference and signal arms. The linear stages move the goniometers in the signal arm to illuminate the target hogel t_i. The ray passes through the reflective collimator and is propagated in a specific direction θ by the goniometers. In the reference arm, the configuration of the reference beam is almost the same as that of the signal arm, except for the goniometer, and the reference beam has a fixed angle. The tilting angle of the reference beam is adjustable using the collimator mount socket. The linear stages also change the illumination position of the reference beam with respect to hogel t_i, as shown in Figure 3b. The hologram material is positioned between the two collimators. Figure 3c shows a photograph of the hologram printer used to fabricate the correct HOE to the speckle noise-free IHP. Figure 3d shows the light source parts. As the light source, a pig-tailed laser (Cobolt 04 series of 532 nm and 100 mW) is used. Light from the laser is briefly exposed to the free space in a fiber-to-fiber U-bench (FBP-A-FC, Thorlabs). An optical shutter (SH1/M, Thorlabs) is also installed in the U-benches, which blocks the beam when the printer head moves from one hogel to the next. When the light passes from the U-bench to the fiber optics, it is divided into two fibers, using a 1:2 coupler. Two fibers are connected to two collimators. The collimator, RC02APC-P01 is manufactured by Thorlabs. The linear stage used in this hologram printer is LTS-300/M (Thorlabs), and the total stroke is 300 mm. A goniometer is provided by Newports, and BGS80CC and BGS50CC are assembled for tilting the heads. The tilting angles of the goniometers are $\pm 45°$and $\pm 30°$, respectively.

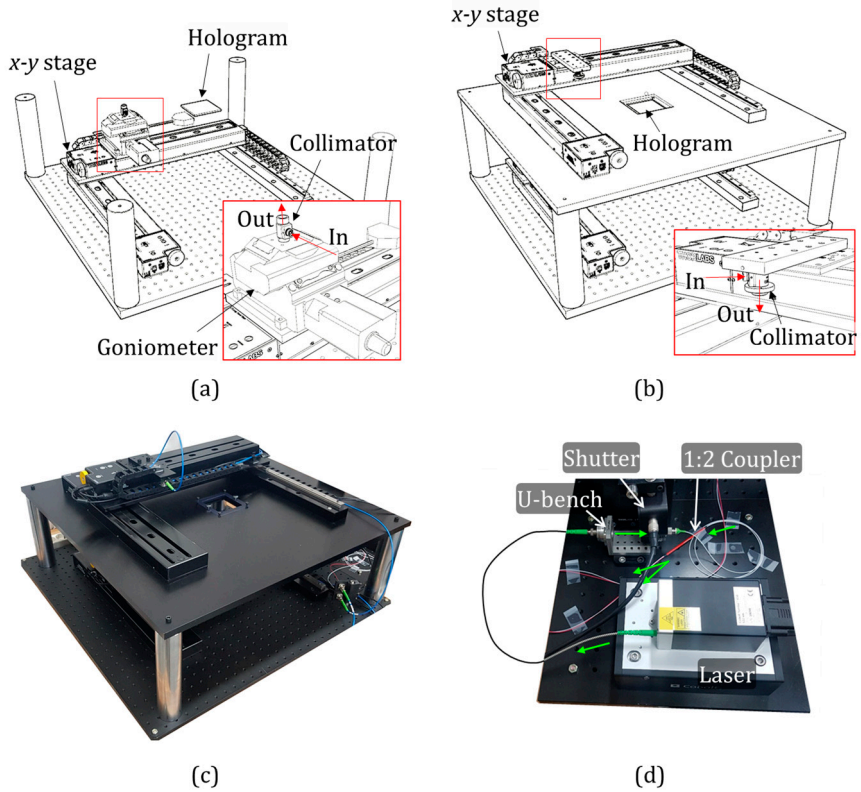


Figure 3. The hologram printer used to generate the HOE for the IHP. Designs of (**a**) signal arm and (**b**) reference arm. Photos of (**c**) the hologram printer and (**d**) light source parts of the realized system.

3. Multi-Depth Projection Based on Interconnective Holographic Projection

Generally, the beam divergence from a laser source depends on the beam width W. The beam divergence angle is formulated as $\theta = \lambda/\pi W$. The reflective collimator used in the hologram printer masks a beam diameter approximately 0.5 mm. In this case, the beam divergence is approximately 0.02°. Figure 4 shows the simulation results of the beam divergence. The simulation is conducted using the angular spectrum method of the

wave propagation [19]. The initial beam diameter is approximately 0.457 mm (D_0). It is observed that the beam width increases very slowly up to 0.5 mm (D_1) at 400 mm and then increases with a divergence angle of 0.025° after that. The maximum projection distance is determined as approximately 1.5 m. This value is the same as the distance at which the beam width is doubled when the pitch of the points comprising images is the same. In this study, we set the IHP range from zero to 400 mm because this range maximizes the contrast of the points comprising the projected images. Therefore, the resolving power of the projected image is set to 0.5 mm.

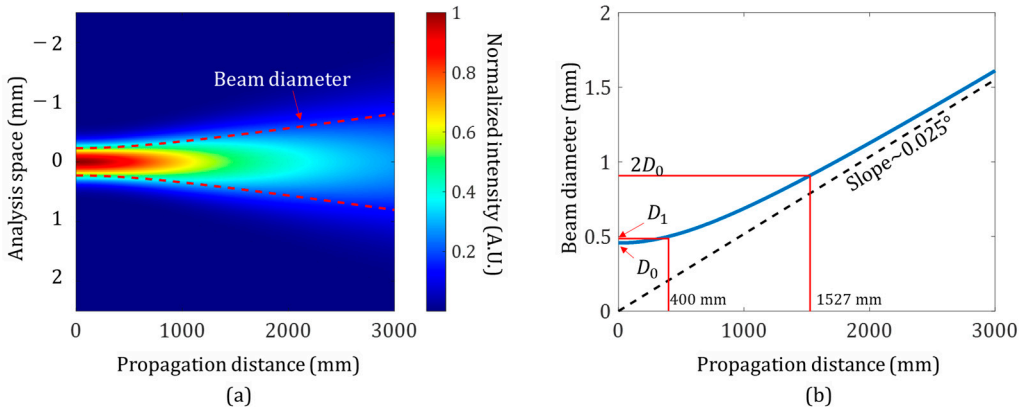


Figure 4. Simulation results of collimated beam propagation. (**a**) Normalized intensity and (**b**) beam diameter per propagation distance.

Figure 5 shows the proposed scheme of the IHP on multi-depth planes. In particular, Figure 5a,b represent two different cases, the collimated and diverging projections. T is a set of hogels, and A and B are the sets of points consisting of two sequential images, respectively. In this study, A and B are represented as two icons: a human head and a light bulb, respectively. The incident beam at point t_i on the hologram is diffracted and heads to point b_i, on plane z_2, after passing through point a_i, on plane z_1. To achieve a 1:1:1 interconnection among a hogel, and each point on the two images, the algorithm is written in the tables below.

Algorithm 1 suggests several possible interconnection combinations as $n \times m \times k$ matrices. It determines the possible interconnection between two points on each image plane. Additionally, it excludes combinations in which the slope of the straight line containing two points is greater than the tilting angle expressed by the goniometer meter. Algorithm 2 chooses a combination of possible features. In Algorithm 2, $\boldsymbol{P}$ indicates the number of connections.

Figure 6 shows the geometric relation between the rotation angles around the x- and y-axes and the tilting angles of the upper and lower goniometers used for the hologram printer. It needs to be transformed into correct angle values for the goniometers. The rotation angles around the x- and y-axes are defined as follows:

$$tan\varnothing_x = \frac{a_{i,x}}{a_{i,z}} \tag{3a}$$

$$tan\varnothing_y = \frac{a_{i,y}}{a_{i,z}} \tag{3b}$$

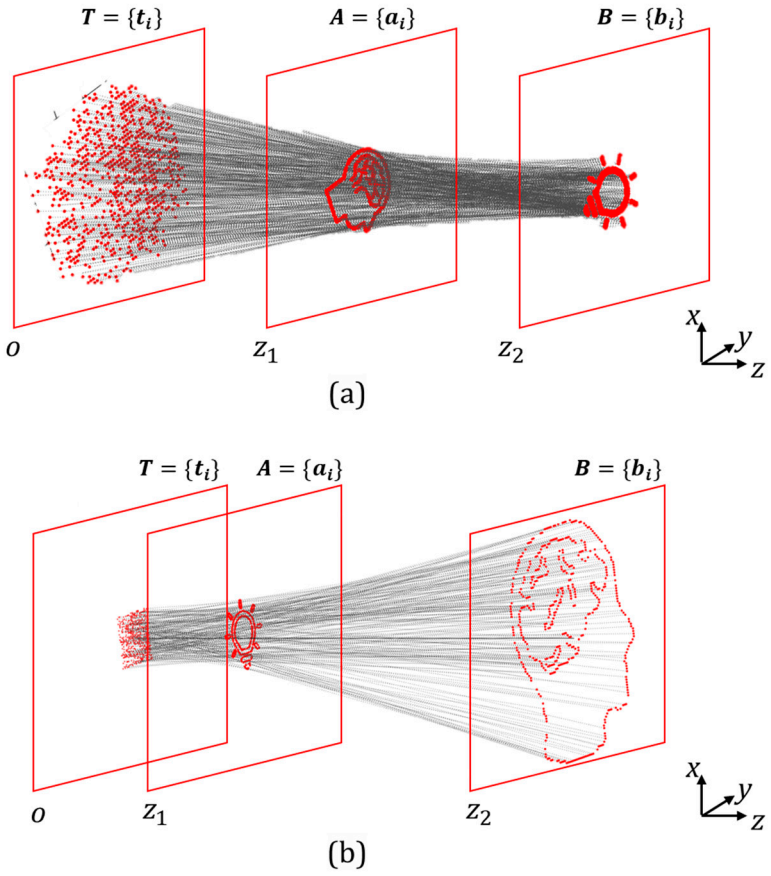


Figure 5. Proposed speckle noise-free interconnective holographic projection on multi-depth planes. (**a**) Collimated interconnective holographic projection and (**b**) diverging interconnective holographic projection.

Algorithm 1: Count optical interconnection combination.

Inputs:
A $= \{\boldsymbol{a}_i\} = \{(x,y)\}$, B $= \left\{\boldsymbol{b}_j\right\} = \{(x,y)\}$,
T $= \{t_k\} = \{(x,y)|$ *x and y are smaller than the size of HOE*$\}$
Initialize:
let $\boldsymbol{H}$ be a new $|A| \times |B| \times |T|$ Matrix
let $\boldsymbol{p}$ be a temporal array (x,y)
Output:
The number of the interconnection $\boldsymbol{H}$
while i $< |A|$
  while j $< |B|$
    $\boldsymbol{p}$ is the intersection of a straight line connecting two points
    if the slope of the line is larger than goniometer titling angle
      continue
    end
    $k \leftarrow$ Get index of nearest point t_k with $\boldsymbol{p}$
    $h_{i,j,k} += 1$
  end
end
Return $\boldsymbol{H}$

Algorithm 2: Get Interconnection Matrix.

Inputs:
$\boldsymbol{H}$, A, B, T
Initialize:
m is the total number of interconnections
let $\boldsymbol{C}$ be a new $|A| \times |B| \times |T|$ Matrix
$\boldsymbol{P}^T \leftarrow \sum_{\boldsymbol{i}}^{|\boldsymbol{A}|} \sum_{\boldsymbol{j}}^{|\boldsymbol{B}|} \boldsymbol{H}$
Output:
Connection matrix, $\boldsymbol{C}$

while $\sum_k^{|T|} P^T > 0$
  $k_M \leftarrow \text{argmax}\{P^T\}$
  $\boldsymbol{P}^A \leftarrow \sum_{\boldsymbol{i}}^{|\boldsymbol{B}|} \boldsymbol{H}_{k=k_M}$
  $\boldsymbol{P}^B \leftarrow \sum_{\boldsymbol{i}}^{|\boldsymbol{A}|} \boldsymbol{H}_{k=k_M}$
  i or j $\leftarrow \text{argmax}\left[min\left\{\boldsymbol{P}^A, \boldsymbol{P}^B\right\}\right]$
  find j of which $\boldsymbol{b}_j$ is interconnected with $\boldsymbol{a}_i$
  $c_{i,j,k} = 1$
end
Return $\boldsymbol{C}$

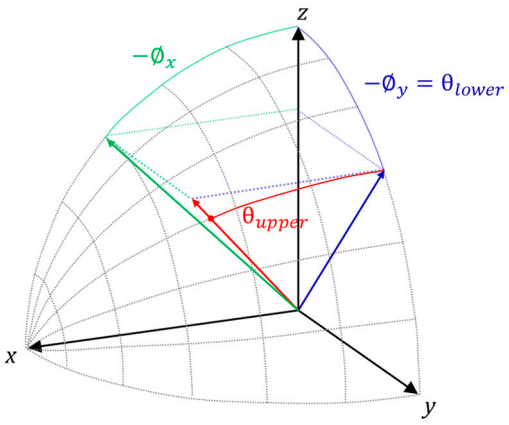


Figure 6. Geometric relation between the rotation angles around the x- and y-axes and tilting angles of the upper and lower goniometers.

In the hologram printer, two goniometers are combined to rotate the incident rays. The tilting angles of the upper and lower goniometers are not equal to the rotation angles around the x- and y-axes. The tilting angles θ_{lower} and θ_{upper} of the goniometers are obtained using a rotation matrix, as follows:

$$tan\theta_{lower} = \frac{sin\varnothing_y}{cos\varnothing_x cos\varnothing_y} \tag{4a}$$

$$tan\theta_{upper} = -\frac{sin\varnothing_x}{cos\varnothing_x} \tag{4b}$$

4. Experimental Results

In general, the holographic optical element has an inevitable direct current (DC) noise that is an unmodulated term. To avoid this DC noise, the direction of the reference beam in the hologram printer was tilted approximately 30° from the normal vector of the HOE. Figure 7 shows the experimental results for the proposed speckle noise-free IHP. The size of the HOE is 50 × 50 mm^2 and the number of hogels identifying connectivity is 668. Here, z_1 and z_2 are set to 100 and 400 mm, respectively. In the record parameters, the hogel pitch is set to 0.5 mm, and the dot pitch in both z_1 and z_2 is 0.5 mm. The icon sizes are designed

differently depending on the depth. Here, the size of the light bulb at z_1 is approximately 30×30 mm^2, and the size of the human head at z_2 is approximately 90×90 mm^2. As shown in Figure 7a, the collimated green laser illuminates the HOE at an angle of 30° oblique. Then, the recorded hogel diffracts the incident beam, and the diffracted rays connect the dots comprising the icons at the target depth planes. The connected dots are sufficiently well arranged to represent the light bulb icon, as shown in Figure 7b. The observed icon is the same size as that of the simulation. The human head icon is also well represented by connected dots when the screen is positioned at z_2, as shown in Figure 7c.

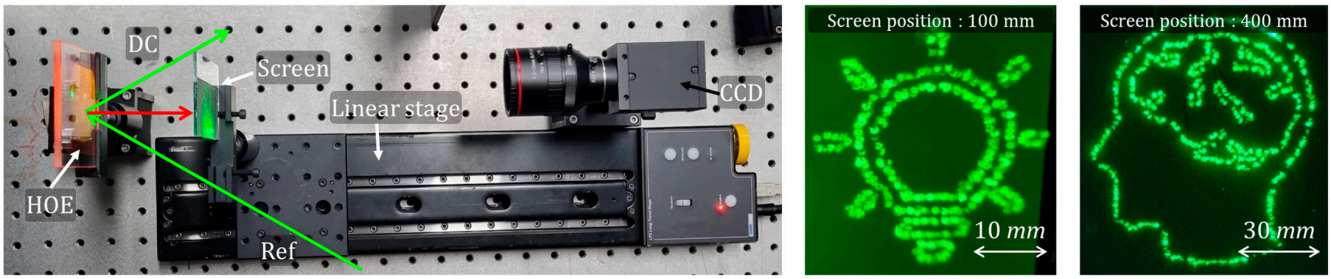


Figure 7. Experimental result for speckle noise-free interconnective holographic projection with icons having different sizes and positions (Video S1: visualization 1). (**a**) Experimental set up, (**b**) the human head icon at z_1, and (**c**) the light bulb icon at z_2.

Figure 8 shows the experimental results demonstrating the holographic optical interconnection in the near field. The parameters are almost the same as those used in the previous experiment. The size of the HOE is 50×50 mm^2, and the hogel and dot pitch are 0.5 mm. The size of the icon is 20×20 mm^2. The number of connections is 321. z_1 and z_2 are set to 50 and 100 mm, respectively. As shown in Figure 8a, the green laser is reflected by the mirror and collimated by a collimation lens, and the collimated beam illuminates the HOE at an angle of 30° oblique. As shown in Figure 8b, the human head is clearly observed where the screen is positioned at z_1. A light bulb is also formed at z_2, as shown in Figure 8c. This result demonstrates that the proposed method connects the two depths. The icons are formed owing to the well-separated dots.

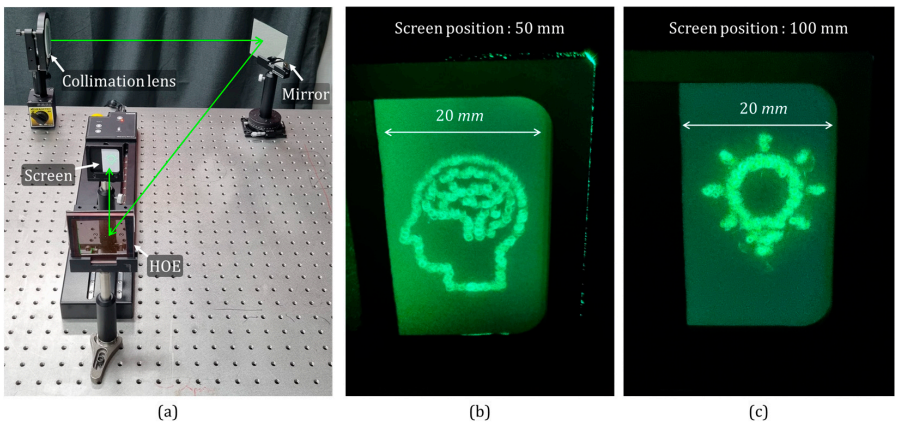


Figure 8. Experimental results for short throw interconnective holographic projection (Video S2: visualization 2). (**a**) Experimental set up and observation for (**b**) the human head icon at z_1 and (**c**) the light bulb icon at z_2.

5. Discussion

We propose a speckle noise-free IHP based on optical interconnections. The proposed method connects two points by changing the direction of the incident rays, through diffraction from a linear grating recorded on a holographic medium. It eliminates speckle and

crosstalk noise by connecting two points using the low divergence of a Gaussian beam. Even though there is no clear limit, the connection of more than two images is much more difficult to solve. If the number of dots to be connected is too large, it is impossible to find a solution to connect the entire dots exclusively. Figure 9 shows the simulation results comparing the binary hologram method [17] with the proposed methods. Figure 9a shows the desired signal distribution; the signal distributions are distinguished by blue and red lines based on each depth z_1 and z_2. Figure 9b shows the simulation results obtained using the binary-phase hologram method. The simulation is conducted with a 0.3 µm pixel pitch. The signal distributions at each depth plane almost resemble the desired signal. However, owing to the random noise of the phase-modulation method, the signal-to-noise ratio is as low as 5 dB.

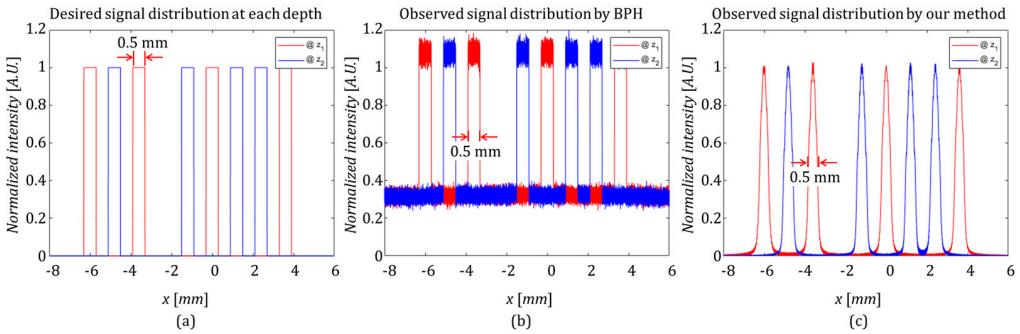


Figure 9. Simulation for holographic optical interconnections. (**a**) Desired signal distribution at each depth, simulation result for (**b**) the binary-phase hologram method and (**c**) the proposed method. (Red and blue line indicates the signal distribution at $z_1 = 15$ mm and $z_2 = 30$ mm, respectively).

On the contrary, the proposed method shows a high signal-to-noise ratio of 15 dB under the same conditions owing to the low divergence of the light. The fabrication process is then simplified using the proposed hologram printer. We expect that our method will contribute to high-contrast holographic projections.

6. Conclusions

In holographic projection, the speckle noise with an undesirable high spatial frequency is considered unavoidable. The speckle noise typically reduces the contrast of a projection image. In this study, we propose a novel holographic optical interconnection method by interconnecting two points in pairs where the points comprise the projection images. The HOE is recorded by interfering with two Gaussian beams with low divergence. As the reconstructed beam from the HOE propagates with a small divergence angle, projection images are formed without speckle noise. The simulation results show that the proposed method has a larger signal-to-noise ratio of 10 dB compared to the conventional method. Experimentally, we demonstrated speckle-free interconnectivity, forming two images at different depths by connecting the points comprising the images. Experiments were conducted under two conditions: diverging and collimated projections. Two HOEs were fabricated using a hologram printer specially designed for optical interconnection. In the future, we will improve the system to include degrees of freedom, not only in the incident angle of the object beam, but also the incident angle of the reference beam. Therefore, it is possible to fabricate HOEs suitable for various reconstruction conditions with different reference beam convergence angles. The proposed method will potentially be useful for optical interconnection and holographic image projection.

Supplementary Materials: The following supporting information can be downloaded at: https://www.mdpi.com/article/10.3390/photonics9120899/s1, Video S1: Visualization 1. Video S2: Visualization 2.

Author Contributions: Conceptualization and methodology, H.J. and J.H.; formal analysis and validation, H.J.; writing—original draft preparation, H.J.; supervision, J.H. All authors have read and agreed to the published version of the manuscript.

Funding: KEIT (1415179744), MOTIE (20019169).

Institutional Review Board Statement: Not applicable.

Informed Consent Statement: Not applicable.

Data Availability Statement: Not applicable.

Acknowledgments: This work was supported by an Alchemist Project grant funded by the Korea Evaluation Institute of Industrial Technology (KEIT) and the Korean Government (MOTIE) (Project Numbers: 1415179744 and 20019169).

Conflicts of Interest: The authors declare no conflict of interest.

References

1. Takahashi, T.; Shimobaba, T.; Kakue, T.; Ito, T. Time-division color holographic projection in large size using a digital micromirror device. *Appl. Sci.* **2021**, *11*, 6277. [CrossRef]
2. Jiao, S.; Zhang, D.; Zhang, C.; Gao, Y.; Lei, T.; Yuan, X. Complex-amplitude holographic projection with a digital micromirror device (DMD) and error diffusion algorithm. *IEEE J. Sel. Top. Quantum Electron.* **2020**, *26*, 1–8. [CrossRef]
3. Makowski, M.; Ducin, I.; Kakarenko, K.; Suszek, J.; Sypek, M.; Kolodziejczyk, A. Simple holographic projection in color. *Opt. Express* **2012**, *20*, 25130–25136. [CrossRef] [PubMed]
4. Qu, W.; Gu, H.; Tan, Q. Holographic projection with higher image quality. *Opt. Express* **2016**, *24*, 19179–19184. [CrossRef] [PubMed]
5. Moon, W.; Jeon, H.; Park, S.; Kim, S.; Kim, H.; Hahn, J. Seamless holographic image generation for a multi-vision system. *J. Inf. Disp.* **2022**, *23*, 1–12. [CrossRef]
6. Min, K.; Park, J.H. Quality enhancement of binary-encoded amplitude holograms by using error diffusion. *Opt. Express* **2020**, *28*, 38140–38154. [CrossRef]
7. Mugeon, K.; Sungjin, L.; Geunseop, C.; Youngmin, K.; Hwi, K.; Joonku, H. Expanded exit-pupil holographic head-mounted display with high-speed digital micromirror device. *ETRI J.* **2018**, *40*, 366–375.
8. Park, S.; Lee, J.; Lim, S.; Kim, M.; Ahn, S.; Hwang, S.; Kim, H. Wide-viewing full-color depthmap computer-generated holograms. *Opt. Express* **2021**, *29*, 26793–26807. [CrossRef] [PubMed]
9. Daeho, Y.; Wontaek, S.; Hyeonseung, Y.; Sun Il, K.; Bongsu, S.; Chang-Kun, L.; Seokil, M.; Jungkwuen, A.; Jong-Young, H.; Geeyoung, S.; et al. Diffraction-engineered holography: Beyond the depth representation limit of holographic displays. *Nat. Commun.* **2022**, *13*, 6012.
10. Qi, Y.; Chenliang, C.; Jun, X. Speckleless holographic display by complex modulation based on double-phase method. *Opt. Express* **2016**, *24*, 30368–30378. [CrossRef] [PubMed]
11. Lee, B.; Kim, D.; Lee, S.; Chen, C.; Lee, B. High-contrast, speckle-free, true 3D holography via binary CGH optimization. *Sci. Rep.* **2022**, *12*, 2811. [CrossRef]
12. Lim, S.; Jeon, H.; Ahn, S.; Hahn, J. Optimal Spatial Coherence of a Light-Emitting Diode in a Digital Holographic Display. *Appl. Sci.* **2022**, *12*, 4176. [CrossRef]
13. Li, H.; Lee, W.B.; Zhou, C.; Choi, D.Y.; Lee, S.S. Flat retroreflector based on a metasurface doublet enabling reliable and angle-tolerant free-space optical link. *Adv. Opt. Mater.* **2021**, *9*, 2100796. [CrossRef]
14. Wippermann, F.; Radtke, D.; Amberg, M.; Sinzinger, S. Integrated free-space optical interconnect fabricated in planar optics using chirped microlens arrays. *Opt. Express* **2006**, *14*, 10765–10778. [CrossRef] [PubMed]
15. Yang, Y.; Wang, J. Cost-effective designs of WDM optical interconnects. *IEEE Trans. Parallel Distrib. Syst.* **2005**, *16*, 51–66. [CrossRef]
16. Kostuk, R.K.; Goodman, J.W.; Hesselink, L. Design considerations for holographic optical interconnects. *Appl. Opt.* **1987**, *26*, 3947–3953. [CrossRef] [PubMed]
17. Suh, H.H.; Kwak, C.H.; Lee, E.H. Combined binary-phase holograms for free-space optical interconnection. *Opt. Lett.* **1995**, *20*, 2131–2133. [CrossRef] [PubMed]
18. Georgiou, A.; Beeckman, J.; Neyts, K. Multicasting optical interconnects using liquid crystal over silicon devices. *J. Opt. Soc. Am. A* **2011**, *28*, 363–372. [CrossRef] [PubMed]
19. Goodman, J.W. *Introduction to Fourier Optics*, 3rd ed.; Roberts and Company Publishers: Englewood, CO, USA, 2005; pp. 208–210.
20. Jeon, H.; Lim, S.; Jeon, Y.; Baek, W.; Heo, D.; Kim, Y.; Kim, H.; Hahn, J. Holographic printing for generating large-angle freeform holographic optical elements. *Opt. Lett.* **2022**, *47*, 257–260. [CrossRef] [PubMed]